Progress In Electromagnetics Research, PIER 61, 143–158, 2006

EXPERIMENTAL ANECHOIC CHAMBER MEASUREMENTS OF A TARGET NEAR AN INTERFACE

N. P. Marquart

German Aerospace Center (DLR)
Microwave and Radar Institute
Münchnerstr. 20, 82230 Wessling, Germany

Abstract—The backscattered field of an illuminated sphere with diameter $\varnothing = 30.5\,\mathrm{cm}$ above a perfect conducting plate is measured in an anechoic chamber at different heights for a varying incidence angle ϕ in the range 5° to 75°. A high frequency field $\lambda \ll \varnothing$ is transmitted, so that two significant transitions from lit to shadow regions are given over the entire incidence angle range for the considered ray field. The polarimetric behavior of the measured scattering matrix $[S]$ is investigated by using the common coherent and incoherent decomposition theorems used by the radar polarimetry scientific community. Close to the shadow boundaries the polarimetric behavior of the sphere significantly changes. Representing the different decomposition parameters used in radar polarimetry over the incidence angle range, the transition zones are related to local maxima or minima. Hence, the extreme values of the polarimetric parameters give information about the geometrical parameters e.g target size and its height above the plate.

1. INTRODUCTION

According to the localization principle of the Geometrical Theory of Diffraction (GTD) where $k \to \infty$, a complex shaped target can be locally replaced by canonical objects. For a smooth convex target in front of an interface, the simplest problem is here a sphere or a cylinder. The polarimetric behavior of the sphere or cylinder gives the main features of the polarimetric behavior of any arbitrary convex target. Moreover the GTD field has the same singularities as in the

original problem (caustics, shadow boundaries). In accordance to the GTD the scattered field from a sphere in proximity of an interface of two dielectric half-spaces is described by a ray system consisting of 13 different spatial and creeping waves shown Fig. 3 to 15. The ray system was validated by an exact full wave field solution based on a Method of Moments (MoM) program. The accuracy of the GTD ray system is discussed in details in [1]. Where it is shown that by varying the incidence angle at the target from perpendicular to grazing incidence lit and shadow regions are given in the ray system which depend solely of the geometrical parameters. As outlined in Fig. 20(a), with decreasing look angle Φ, the waves 3 and 8 will approach the shadow boundary (SSB1) on their way back to the receiver and finally are replaced by the wave 4 at the transition. Here the corresponding look angle is given by Φ_1. The wave 4 propagates on a small arc length along the cylinder and compared to the spatial waves 3 and 8 the creeping wave 4 is powerless. The same comments hold for the second considered transition zone at the boundary SSB2 Fig. 20(b). Where by crossing the boundary, the creeping wave 13 replaces the spatial waves 11 and 12 at the incidence angle Φ_2 Incomparison to the first shadow boundary the two waves have here one additional interaction with the cylinder and the interface. Hence, two principal transition zones are given in the ray field for the monostatic alignment of the transmitting and receiving antenna. The transition from the lit to the shadow region modifies the polarimetric behavior of the target significantly. The polarimetric behavior according to the numerical results was investigated at first on the Poincaré sphere and presented in [2]. Where it was shown that the corresponding transition zones have characteristic locations on the Poincaré sphere. In this paper the polarimetric behavior in the above mentioned transition regions for such a setup is investigated by measurements performed in an anechoic chamber. The measured scattering matrix $[S]$ is decomposed after the common decomposition theorems for every single incidence angle. The corresponding polarimetric parameters are plotted over the entire look angle range in order to refined a correlation between the polarimetric parameters and the geometrical shadow boundaries. As a result, the look angles corresponding to the transition regions can be exploited in order to get information about the geometrical properties of the target and its distance to the interface. The controlled in-room measurements are discussed in the following.

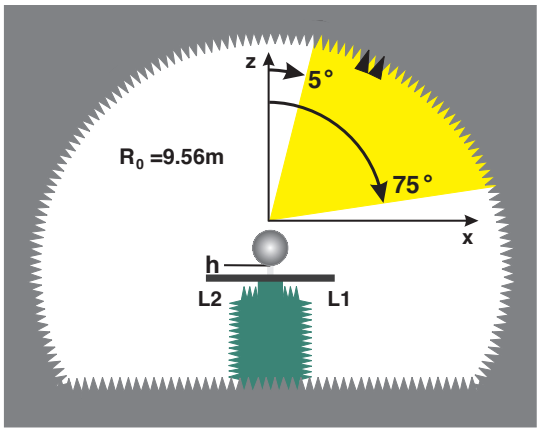

Figure 1. Cross Section EMSL.

2. ANECHOIC CHAMBER SETUP

The diffracted field from a metallic sphere was centered above a perfect conducting plate with the dimension 2 m×2 m. The backscattered field was measured at five different heights: $h = 3.75$ cm, 5.0 cm, 7.5 cm, 10.0 cm and 15.0 cm in the EMSL†. The EMSL provides a 20 m diameter microwave anechoic chamber, where the sphere-metallic plate was scanned over the hemisphere in a monostatic alignment as shown in Fig 1. The look angle ϕ range spanned from 5° to 75° with breakpoints every half degree $\Delta\phi = 0.5°$. At each of the single 140 breakpoints a frequency sweep over the range 1.5 GHz–9.5 GHz with a step of $\Delta f = 10$ MHz was performed. The distance sphere-plate was realized by supports made of polystyrene exemplarily shown for the height $h = 10.0$ cm in Fig. 2. A correction of the raw data was required as systematic errors and residual reflections in the chamber were given during the measurements. In order to neglect this amplitude and phase noise, a three target calibration and error correction for the monostatic alignment was carried out [3]. The data corresponding to the two heights $h = 7.5$ cm and 15.0 cm are presented exemplarily in the following.

† European Microwave Signature Laboratory (EMSL) at the Joint Research Centre (JRC) of the European Commission in Ispra, Italy

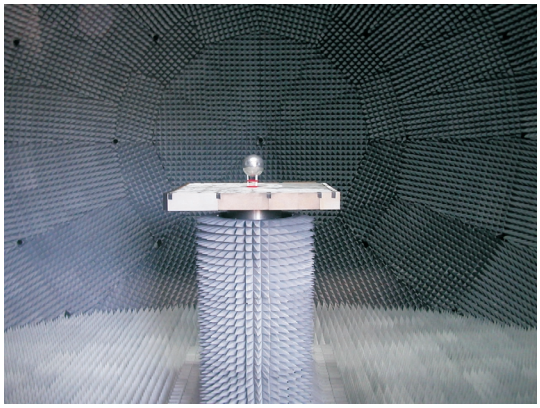

Figure 2. Support of the sphere for height $h = 10\,\text{cm}$.

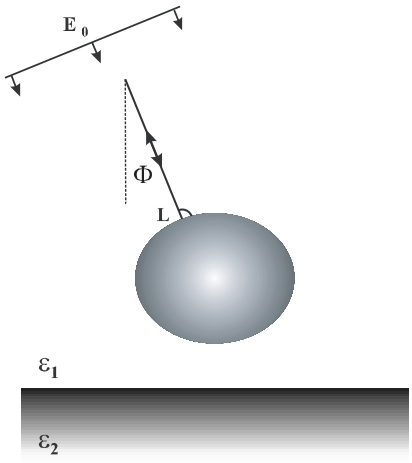

Figure 3. Wave 1 and phase origin.

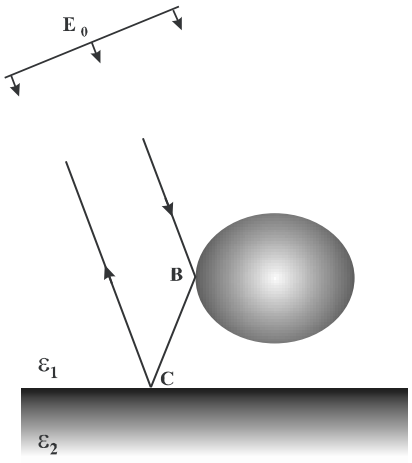

Figure 4. Wave 2 (double bounce).

3. TRANSITION ZONES

At the shadow boundaries the spatial waves disappear and transform into creeping waves which are strongly attenuated on the shadowed side, leading to a rapid loss of power. The direct reflected wave 1 is constant over the whole look angle range and not restricted by any shadow boundary. In this sense wave 1 gives no additional information about the geometrical parameters like the height (h) above

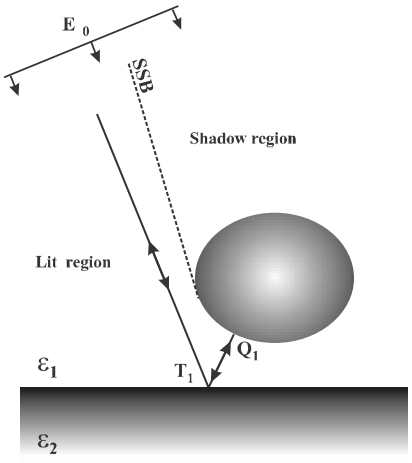

Figure 5. Wave 3.

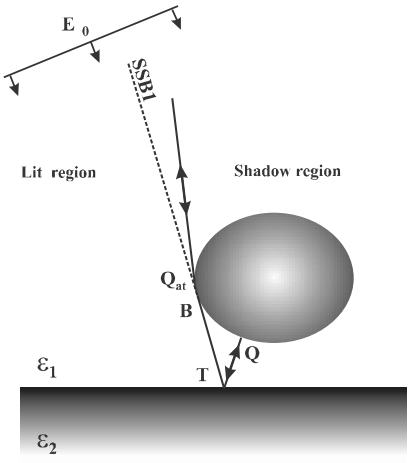

Figure 6. Wave 4.

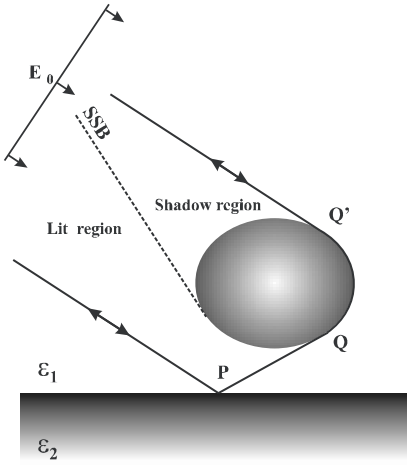

Figure 7. Wave 5.

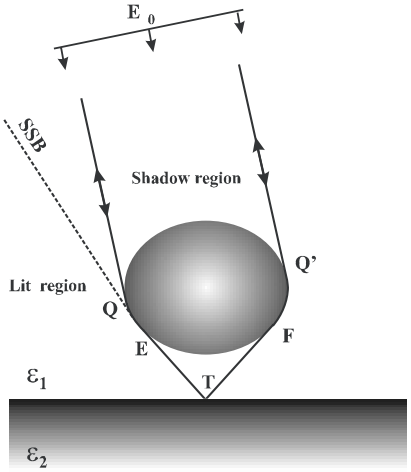

Figure 8. Wave 6.

the interface or the geometrical properties of the sphere. Therefore in order to reinforce the remaining waves of the ray system the contribution of wave 1 is neglected. As a frequency sweep is performed at every look angle a corresponding pulse is given in the time domain. Further, in the time domain the direct reflected wave 1 is the first received signal, so that its contribution can be simply neglected. Going back to frequency domain (e.g., $f = 6.7\,\mathrm{GHz}$) a good agreement

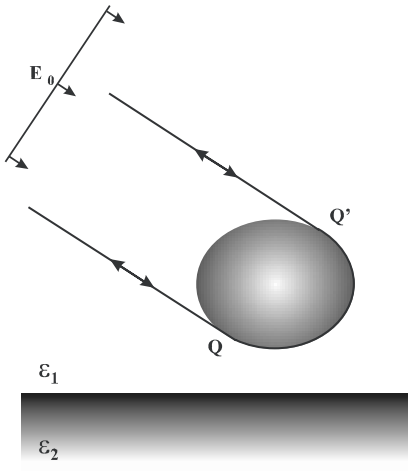

Figure 9. Wave 7 (creeping wave).

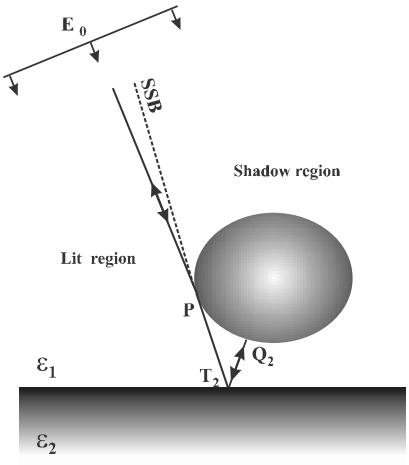

Figure 10. Wave 8.

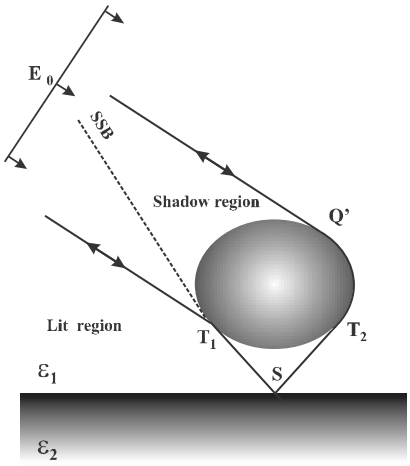

Figure 11. Wave 9.

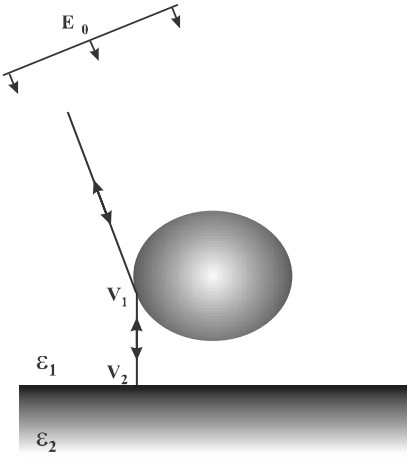

Figure 12. Wave 10.

between the predicted transition zones SSB1 and SSB2 are noticed for all measured heights. Exemplarily the energy depression is pointed out for the heights $h = 7.5\,\text{cm}$ and $15.0\,\text{cm}$ in Fig. 17(a) and 17(b) for the received field without the contribution of the direct reflected wave 1.

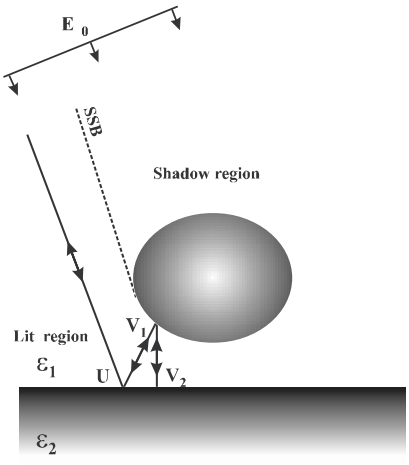

Figure 13. Wave 11.

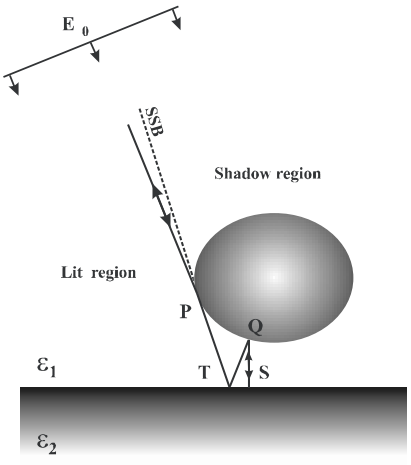

Figure 14. Wave 12.

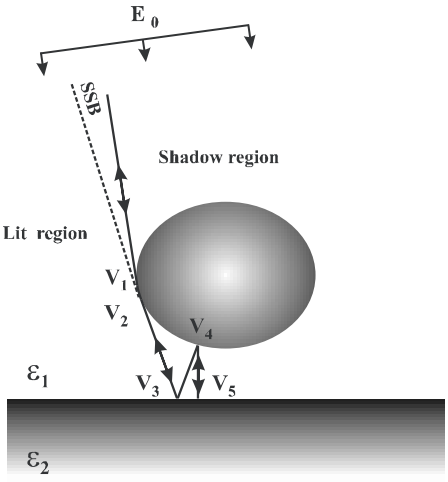

Figure 15. Wave 13.

4. KROGAGER DECOMPOSITION

The Krogagger decomposition considerers coherent reflections during the scattering process. Here, the scattering matrix $[S]$ is decomposed into a sum of three canonical targets namely a sphere, a diplane and a helix. More precisely the corresponding three submatrices represent in fact odd-even bounced interactions and the last term mentioned

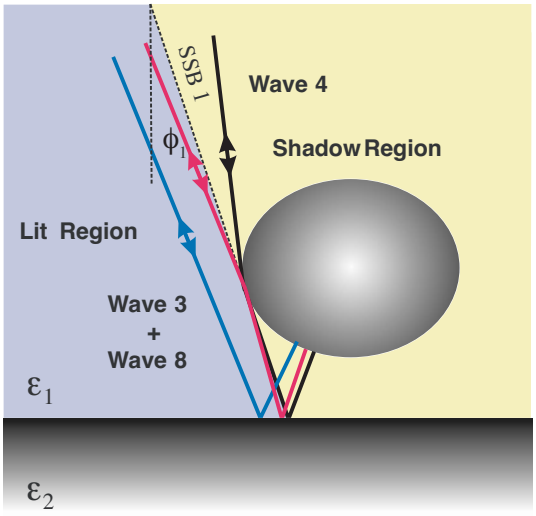

(a) SSB 1

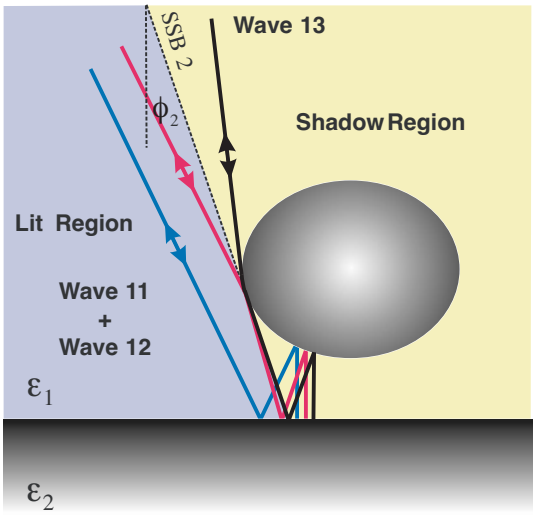

(b) SSB 2

Figure 16. The two principal surface shadow boundaries SSB1 and SSB1 in the backscattered ray field.

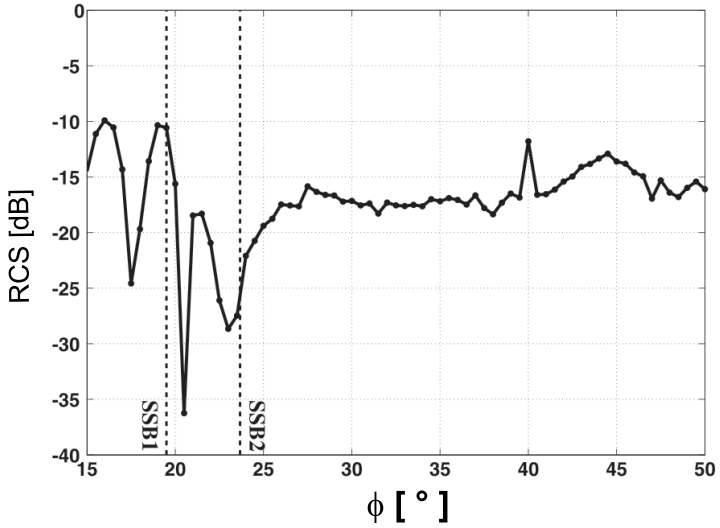

(a) $h = 7.5\,\mathrm{cm}$

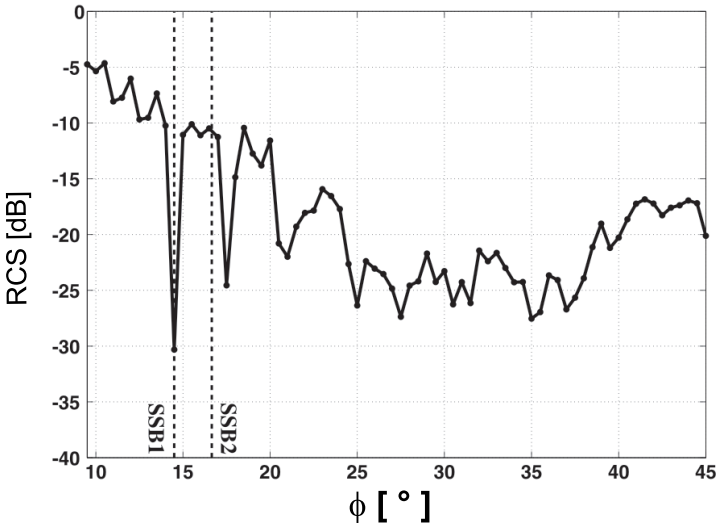

(b) $h = 15.0\,\mathrm{cm}$

Figure 17. Radar Cross Section (RCS) over the look angle range ϕ of the reduced field at $f = 6.7\,\mathrm{GHz}$. The transition zones are pointed out as $SSB1$ and $SSB2$.

as helix term refers to cross-polarization. In the following the total received field is analyzed where the contribution of the the specular wave 1 is included. The coherent decomposition in accordance to Krogager is given by:

$$[S] = |a|\, e^{i\phi_a} \begin{bmatrix} 1 & 0 \\ 0 & 1 \end{bmatrix} + |b|\, e^{i\phi_b} \begin{bmatrix} 1 & 0 \\ 0 & -1 \end{bmatrix} + |c|\, e^{i\phi_c} \begin{bmatrix} 0 & 1 \\ 1 & 0 \end{bmatrix} \quad (1)$$

Rewritten in its final form by [4]:

$$[S] = k_s[S]_{odd} + e^{i\phi_r}\,[k_d[S]_{even} + k_h[S]_{helix}] \quad (2)$$

According to the symmetrical setup in the chamber no significant cross-polarization is measured. Hence the coefficient of the helix term is set equal zero. The remaining coefficients k_s and k_d describing the contribution of odd and even interactions are presented in Fig. 18 over the look angle range at the heights $h = 7.5\,\text{cm}$ and $h = 15.0\,\text{cm}$. The matrix $[S]$ corresponds, close to the shadow boundaries, to a scattering process where odd reflection mechanisms are dominant conform with local maxima. In the transition regions the even reflected spatial waves 3+8 and 11+12 corresponding to the shadow boundaries SSB1 and SSB2 are strongly attenuated and finally replaced by their related creeping waves. Hence, at the two transition zones, the direct odd reflected wave 1 has a more significant contribution to the total field.

5. HUYNEN DECOMPOSITION

In the power domain where an incoherent scattering process is measured the 2×2 Graves power matrix $[G]$ is defined as follows [5]:

$$[G] = [S]^*[S] \quad (3)$$

The diagonal elements of $[G]$ are real where in contrast the cross elements are complex quantities. An eigenvalue analysis of $[G]$ is performed and the corresponding eigenvalues rearranged according to their absolute value ($\Lambda_1 > \Lambda_2$). According to the target decomposition of Huynen, the Euler parameter m related to the real physical target size is given by [6]:

$$m = \sqrt{\Lambda_1} \quad (4)$$

The developing of the parameter m from perpendicular to grazing incidence is pointed out in Fig. 19 for the heights $h = 7.5\,\text{cm}$ and $15.0\,\text{cm}$. The measurements in the anechoic chamber show that for

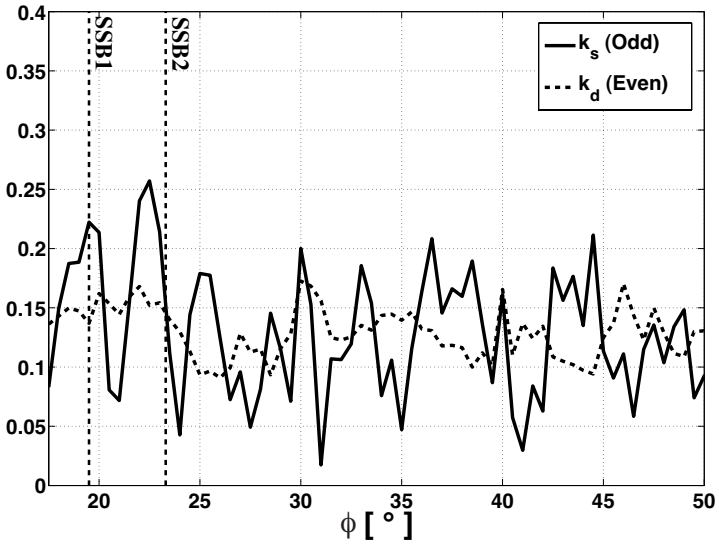

(a) $h = 7.5\,\mathrm{cm}$

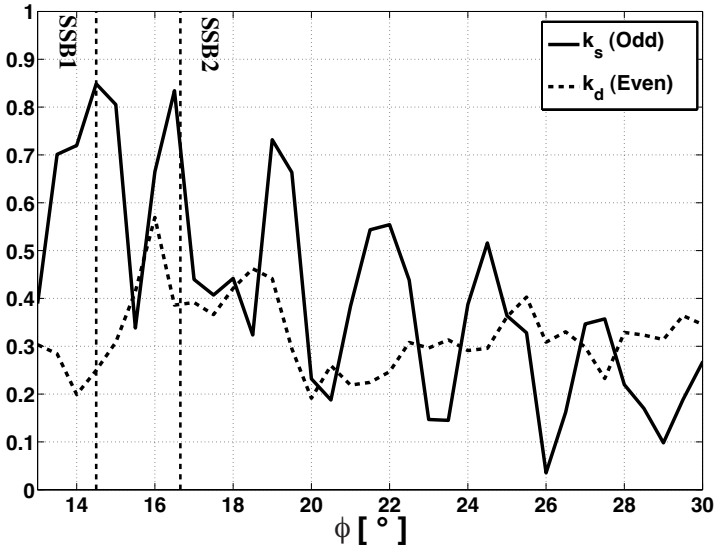

(b) $h = 15.0\,\mathrm{cm}$

Figure 18. Krogager's odd and even reflection coefficients k_s and k_d of the total field $f = 6.7\,\mathrm{GHz}$ over the range of the look angle ϕ.

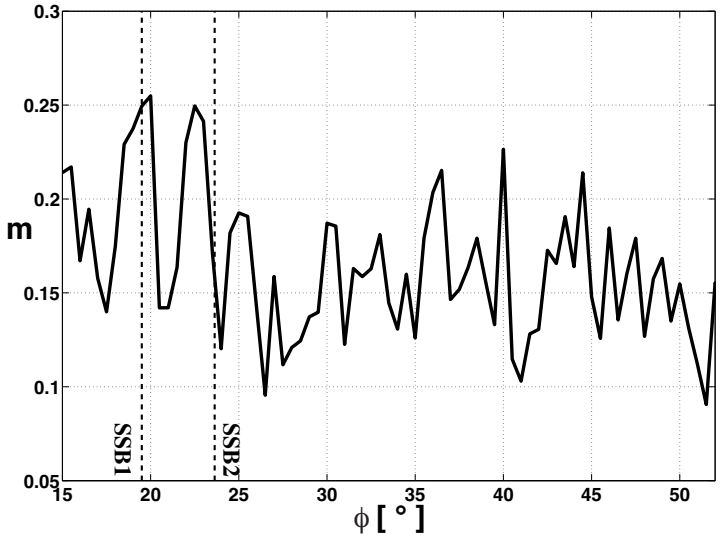

(a) $h = 7.5\,\mathrm{cm}$

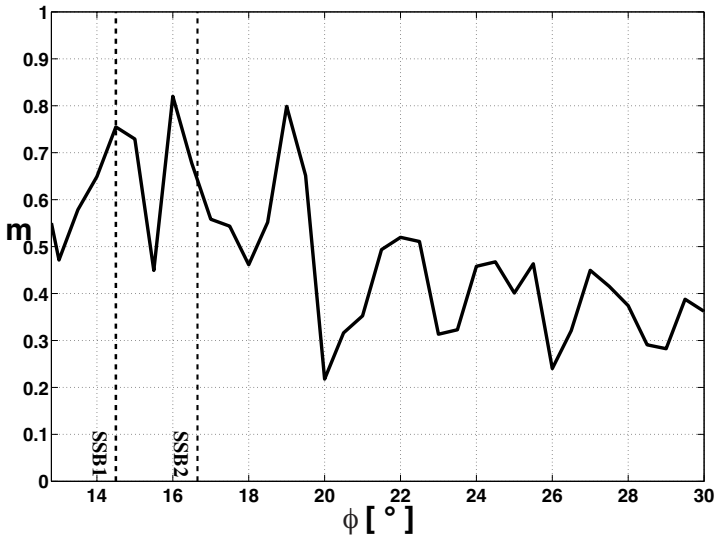

(b) $h = 15.0\,\mathrm{cm}$

Figure 19. Huynen's target size parameter m for different look angles ϕ for the heights $h = 7.5\,\mathrm{cm}$ and $15\,\mathrm{cm}$ at the frequency $f = 6.7\,\mathrm{GHz}$.

all measured heights the two principal shadow boundaries SSB1 and SSB2 correspond to local maxima of the target size parameter m. Due to the strong attenuation of the spatial waves at the transition, the contribution of the specular wave 1 is reinforced, signifying here a bigger object.

6. EIGENVALUE DECOMPOSITION

Another decomposition theorem describing an incoherent scattering process is based on the eigenvalue analysis. In the case where the illuminated area represents a homogenous Gaussian distributed medium, the averaged coherency matrix $\langle[T]\rangle$ carries all the information about the scattering process. In the anechoic chamber setup a symmetry is given around the line of sight, so that the decomposition of $\langle[T]\rangle$ may be written in the form:

$$\langle[T]\rangle = [U_2] \begin{bmatrix} \lambda_1 & 0 \\ 0 & \lambda_2 \end{bmatrix} [U_2]^{*T} \tag{5}$$

In the case that no averaging processes (spatial and temporal) are given during the scattering process only a single non-zero eigenvalue remains, leading [7, 8]:

$$[T] = [U_2] \begin{bmatrix} \lambda_1 & 0 \\ 0 & 0 \end{bmatrix} [U_2]^{*T} \tag{6}$$

In consequence only a single eigenvector remains, given by:

$$\begin{pmatrix} |e_1| \\ |e_2|e^{i\delta} \end{pmatrix} = \begin{pmatrix} \cos\alpha \\ \sin\alpha e^{i\delta} \end{pmatrix} \tag{7}$$

No polarimetric entropy is on hand ($H = 0$) and referring to equation (7) the angle α represents the internal degree of freedom of the illuminated scene. The parameter α runs in the range $0° \leq \alpha \leq 90°$ where at $\alpha = 0°$ odd bounce mechanisms are described furthermore at $\alpha = 45°$ dipole reflections and at $\alpha = 90°$ even bounce interactions are determined. The diagram of the target angle α is outlined for the heights $h = 7.5\,\text{cm}$ and $15\,\text{cm}$ over the look angle range in Fig. 20. Similar to the coherent Krogager and incoherent Huynen decomposition the transition zones corresponds to an odd bounce mechanism (sphere) than to an even bounce mechanism (diplane). This behavior is reflected in local minima of the parameter α. Here the related spatial waves are strongly attenuated and the contribution of the specular wave 1 is in consequence fortified.

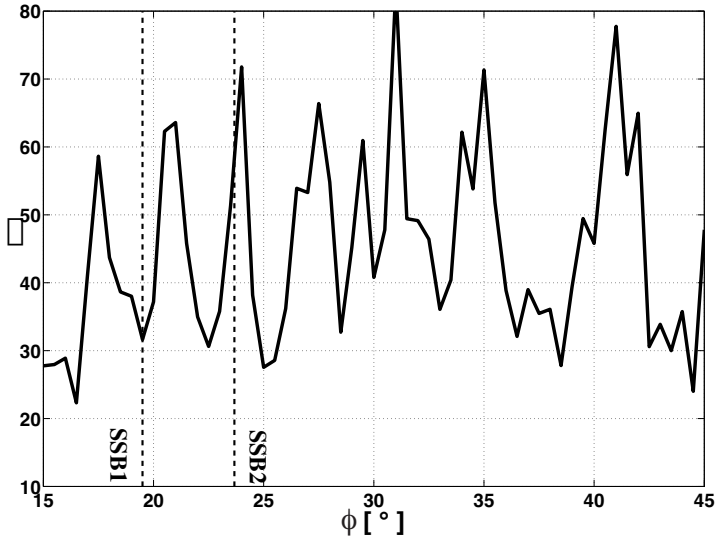

(a) $h = 7.5\,\mathrm{cm}$

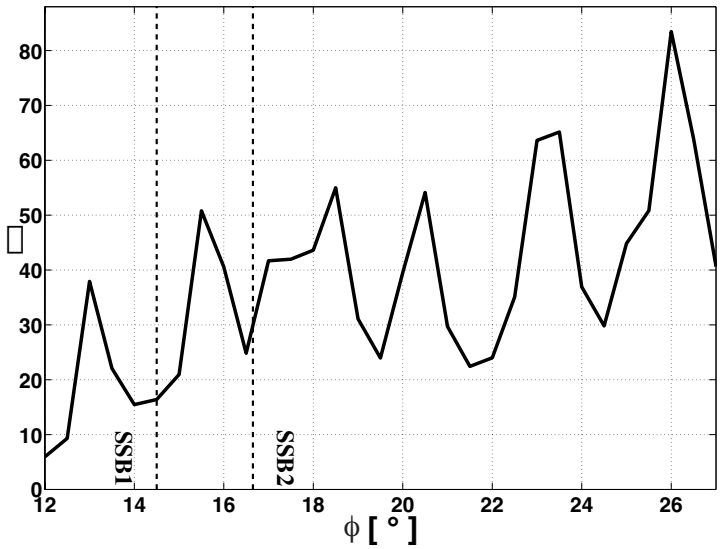

(b) $h = 15.0\,\mathrm{cm}$

Figure 20. Target parameter α of the eigenvalue based decomposition of the total field the frequency $f = 6.7\,\mathrm{GHz}$.

7. CONCLUSION

Monostatic measurements were performed for a metallic sphere centered above a perfect conducting interface at different heights in an anechoic chamber. According to the introduced ray system a special emphasis was attributed to the transition regions, near the geometrical surface shadow boundaries, where the reflected spatial waves disappear and transform into creeping waves at the target which are strongly attenuated on the shadowed side. The transition from the lit to the shadow region and the related energy loss of the backscattered field was confirmed by the measurements. The data were applied to different decomposition theorems commonly used in Radar polarimetry. The coherent decomposition theorem after Krogager into odd, even and helix reflections showed that at the surface shadow boundaries the object appears as a sphere corresponding to local maxima values of k_S. According to incoherent decomposition, the theorem after Huynen showed that at the boundaries the target size m corresponds to local maxima. This agrees with the strong attenuation of the spatial waves at the transition. Finally, according to the eigenvalue decomposition after Cloude and Pottier for the deterministic situation here, no entropy $H = 0$ occurs and a single eigenvector is given. The target parameter α of the eigenvector lies for the different measured heights in the range of $10^\circ < \alpha < 35^\circ$ at the boundaries. This corresponds rather to an odd reflection from a sphere.

ACKNOWLEDGMENT

The authors would like to thank Dr. J. Fortuny and Alberto Martinez from the IPSC at the Joint Research Center from the European Commission in Ispra, Italy.

REFERENCES

1. Marquart, N. P., "Investigation on the polarimetric behavior of the em-field scattered by an object located near the interface between the air and a lossy dielectric half-space," Univ. of Rennes 1, Institute of Electronique and Telecommunications of Rennes, 263, av. du Générale Leclerc, 35042 Rennes Cedex, France, 2006.
2. Marquart, N. P. and F. Molinet, "Polarimetric properties of an object in front of the air-ground interface," *Journal of Electromagnetic Waves and Applications*, 2006.
3. Wiesbeck, W. and D. Kähny, "Single reference, three target calibration and error correction for monostatic, polarimetric free

space measurements," *Proceedings of the IEEE*, Vol. 79, No. 10, 1551–1558, 1991.

4. Krogager, E., "Aspects of polarimetric radar imaging," Danish Defence Research Establishment, Ph.D., 1993.
5. Graves, C. "Radar polarization power matrix," *Proceeding of the IRE*, Vol. 44, 248–252, Feb. 1956.
6. Huynen, J. R., "Phenomenological theory of radar targets," Technical University Delft, Ph.D., Drukkerij Bronder-Offset, NV Rotterdam, The Netherlands, 1970.
7. Cloude, S. and E. Pottier, "A review of target decomposition theorems in radar polarimetry," *IEEE Transactions on Geoscience and Remote Sensing*, Vol. 34, 498–518, Mar. 1996.
8. Cloude, S. and E. Pottier, "An entropy based classification scheme for land applications of polarimetric SAR," *IEEE Transactions on Geoscience and Remote Sensing*, Vol. 35, 68–78, Jan. 1997.